$S = 1/2$ Square-Lattice Antiferromagnets: (CuX)LaB_2O$_7$ and (CuCl)A_2B_3O$_{10}$ (X = Cl, Br; A = Ca, Sr; B = Nb, Ta)

Hiroshi KAGEYAMA,[1,2] Taro KITANO,[1] Ryu NAKANISHI,[1] Jun YASUDA,[1] Noriaki OBA,[1] Yoichi BABA,[1] Masakazu NISHI,[2] Yutaka UEDA,[2] Yoshitami AJIRO[1] and Kazuyoshi YOSHIMURA[1]

[1]*Department of Chemistry, Graduate School of Science, Kyoto University, Kyoto 606-8502, Japan*
[2]*Institute for Solid State Physics, The University of Tokyo, Kashiwa 277-8581, Japan*

A series of magnetic compounds with the formula (CuX)LaB_2O$_7$ and (CuCl)A_2B_3O$_{10}$ (X = Cl, Br; A = Ca, Sr; B = Nb, Ta) have been prepared through a low-temperature topochemical route starting from nonmagnetic double- ($n = 2$) and triple- ($n = 3$) layered perovskites, respectively. The magnetic susceptibility of these compounds typically exhibits a broad maximum at low temperatures, characteristic of low-dimensional antiferromagnetic compounds. However, depending on the choice of the parameters, X, A, B and n, physical quantities such as the Weiss temperature and the temperature at a maximum susceptibility vary to a great extent, which enables us to study the phase diagram of the $S = 1/2$ frustrated square-lattice antiferromagnets (the so-called J_1-J_2 model). In particular, (CuCl)LaNb$_2$O$_7$, possibly having a ferromagnetic J_1 and an antiferromagnetic J_2, shows a spin-liquid behavior with the spin gap of 27 K.

§1. Introduction

Low-dimensional antiferromagnetic (AFM) quantum spin systems with a spin-singlet ground state and an energy gap in the magnetic excitation spectrum have recently received considerable attention. These features arise from quantum spin fluctuations in low-dimensional structures, as exemplified by the spin-Peierls compound $CuGeO_3$, where the spin-singlet ground state is stabilized by a modulation or doubling of the underlying lattice.[1)] Other spin-gap compounds range from the integer-spin chain (Haldane system) $Ni(C_2H_8N_2)_2NO_2(ClO_4)$[2)] to the two-leg spin ladder $SrCu_2O_3$[3)] and the alternating spin chain $Cu(NO_3)_2{\cdot}2.5H_2O$.[4)] After intensive experimental and theoretical study with corresponding model compounds, it is fair to state that the one-dimensional (1D) case is rather well understood. By contrast, little is known about 2D case. Among 2D models, the $S = 1/2$ frustrated square lattice antiferromagnet (J_1-J_2 model) is of special importance in the light of the relevance to the CuO_2 plane in high-T_c superconducting cuprates along with a pseudo spin-gap behavior.[5)] An interesting phase diagram with unusual ground states is predicted as a function of the ratio J_2/J_1 between the first-nearest-neighbor (J_1) and second-nearest-neighbor (J_2) exchange interactions.[6)−8)] For $0 < J_2/J_1 < 0.38$ a normal Néel order state is the ground state, while for $J_2/J_1 > 0.55$ a collinear order should develop. The most interesting phase, a quantum disordered phase with a finite gap is expected for $0.38 < J_2/J_1 < 0.55$. Three compounds are suggested as prototypes of the J_1-J_2 model with a significant coupling between J_1 and J_2, Li_2VOSiO_4 ($J_1 =$

0.56, $J_2 = 6.3$ K), Li_2VOGeO_4 ($J_1 = 0.82$, $J_2 = 4.1$ K)[9),10)] and $Pb_2VO(PO_4)_2$ ($J_1 = -6$ K, $J_2 = 9.8$ K),[11)] all of which are, however, magnetically ordered at low temperatures. Very recently we have reported that a double-layered Dion-Jacobson phase $(CuCl)LaNb_2O_7$, prepared from the topochemical ion-exchange reaction between $RbLaNb_2O_7$ and $CuCl_2$, is the long-time awaited spin-liquid phase for the J_1-J_2 model.[12)] Magnetic susceptibility of $(CuCl)LaNb_2O_7$ exhibits a thermal-activated behavior. The analysis of the magnetic data together with structural considerations gave a ferromagnetic $J_1(< 0)$, an antiferromagnetic $J_2(> 0)$ and the relation $J_1 + J_2 = 9.6$ K. Moreover, neutron scattering experiments provided explicit evidence for a spin-singlet ground state with an energy gap of 2.3 meV ($\sim$26.7 K). A sizable geometrical frustration was derived from the almost Q independent one-triplet excitation, as in the case of $SrCu_2(BO_3)_2$.[13)] Using the same synthetic strategy, it is possible to obtain a series of $S = 1/2$ square-lattice antiferromagnets $(CuX)A_{n-1}B_nO_{3n-1}$ (X = halogen; A = alkaline earth metal or rare earth metal, B= niobium and tantalum; $n = 2, 3$).[14)−16)] These parameters A, B, X and n may offer effective routes to systematically tune the sign and magnitude of exchange constants, and dimensionality. Our ultimate goal is to reveal the phase diagram for the (quasi 2D) J_1-J_2 model experimentally. In this paper, we report on the structural and magnetic properties of $(CuX)A_{n-1}B_nO_{3n-1}$, some of which have been newly synthesized. It turned out that they indeed exhibit, depending on the tuning parameters, a variety of magnetic behaviors ranging from a long-range ordered to a spin-liquid phases.

§2. Experimental details

For the synthesis of the $n = 2$ members, mother compounds $RbLaB_2O_7$ (B = Nb, Ta) were initially prepared by a solid-state reaction method from Rb_2CO_3 (99.99%, La_2O_3 (99.99%), and B_2O_5 (99.999%). $RbLaB_2O_7$ were mixed with 2-fold molar excess of ultra dry CuX_2 (X = Cl, Br) (99.99%) and then pressed into pellets inside the Ar-filled glove box (MBRAUN). Reaction (1) was carried out in sealed, evacuated ($< 10^{-3}$ Torr) Pyrex tubes at 320 ℃ for one week. Final product was washed with water to eliminate the excess copper chloride and alkali-metal byproduct, and dried at 120 ℃. Similarly, the $n = 3$ members $(CuCl)A_2B_3O_{10}$ (A = Ca, Sr; B = Nb, Ta) were able to obtain but using host compounds $RbA_2B_3O_{10}$. X-ray powder diffraction data were collected on a Mac Science M18XHF diffractometer equipped with a graphite monochromator and Cu $K\alpha$ ($\lambda = 1.5406$ Å). Elemental analysis was carried out by energy dispersive spectroscopy (EDX) on a series of individual crystallines on a JEOL scanning electron microscope (SEM) equipped with an EDAX microanalytical system. Magnetic susceptibility measurements were performed on a powder sample with a superconducting quantum interference device (SQUID) magnetometer (Quantum Design, MPMS) over the temperature range T = 2 – 300 K, typically in an applied field of $H = 0.1$ T.

§3. Structural properties

As shown in Fig. 1, the single-step ion-exchange reaction for the synthesis of, e.g., the $n = 3$ members is expressed as

$$\mathrm{Rb}A_2B_3\mathrm{O}_{10} + \mathrm{CuCl}_2 \rightarrow (\mathrm{CuCl})A_2B_3\mathrm{O}_{10} + \mathrm{RbCl}, \tag{1}$$

which involves the replacement of rubidium cation of the perovskite host by $[\mathrm{CuCl}]^+$. The $S = 1/2$ copper ion is octahedrally coordinated, bridging between apical oxygens from the perovskite layer and surrounded by four chlorines in the CuCl plane. The $\mathrm{CuO}_2\mathrm{Cl}_4$ octahedra corner-share with the $B\mathrm{O}_6$ octahedra of the perovskite slabs while edge-sharing with other $\mathrm{CuO}_2\mathrm{Cl}_4$ octahedra in the ab plane. In the CuCl plane, copper ions form the square lattice, while chlorines are located at the center of the 2NN copper bonds, as shown in Fig. 2. Figures 3 and 4 represent X-ray diffraction patterns at room temperature for $(\mathrm{Cu}X)\mathrm{La}B_2\mathrm{O}_7$ and $(\mathrm{CuCl})A_2B_3\mathrm{O}_{10}$, respectively, relative to those for the mother compounds. All profiles could be readily indexed on tetragonal unit cells and no trace of the impurity phase was found within the experimental resolution of the present experiment. The final products are green and brown for the Cl and Br compounds, respectively. The EDX experiment revealed that no residual alkali metal is present in the products and the Cu : X : A : B compositions were found approximately to be 1 : 1 : 1 : 2 for $n = 2$ and 1 : 1 : 2 : 3 for $n = 3$. As seen in Table I, the spacing between the perovskite layers is expanded significantly on the ion-exchange reaction relative to the starting compounds. For the known compounds unit cells obtained from the analysis are consistent with those reported.[14)−16)] It is to be noted that the A = Sr compounds, $(\mathrm{CuCl})\mathrm{Sr}_2\mathrm{Nb}_3\mathrm{O}_{10}$ and $(\mathrm{CuCl})\mathrm{Sr}_2\mathrm{Ta}_3\mathrm{O}_{10}$, have been obtained for the first time in the present study. The observed diffraction patterns without any extinct reflections are quite similar to those of the known $(\mathrm{CuCl})\mathrm{Ca}_2B_3\mathrm{O}_{10}$ with the space group $P4/mmm$.[15),16)] Therefore it is likely that the all $n = 3$ compounds are isostructural with respect to each other. Reflecting the difference in ionic radius, the replacement of Sr for Ca leads to expansion of the lattice parameters a and c.

Table I. Tetragonal unit cell parameters for the parents and the exchange products.

compounds	a (Å)	c (Å)	cell vol. (Å^3)
$\mathrm{RbLaNb}_2\mathrm{O}_7$	3.884(3)	10.963(2)	165.4
$(\mathrm{CuCl})\mathrm{LaNb}_2\mathrm{O}_7$	3.8773(4)	11.726(2)	176.3
$(\mathrm{CuCl})\mathrm{LaTa}_2\mathrm{O}_7$	3.876(4)	11.739(4)	176.4
$(\mathrm{CuBr})\mathrm{LaNb}_2\mathrm{O}_7$	3.8929(3)	11.690(1)	177.2
$(\mathrm{CuCl})\mathrm{LaTa}_2\mathrm{O}_7$	3.894(1)	11.707(2)	177.5
$\mathrm{RbSr}_2\mathrm{Ta}_3\mathrm{O}_{10}$	3.857(6)	15.044(1)	223.8
$(\mathrm{CuCl})\mathrm{Sr}_2\mathrm{Ta}_3\mathrm{O}_{10}$	3.881(3)	15.996(8)	240.9
$(\mathrm{CuCl})\mathrm{Sr}_2\mathrm{Nb}_3\mathrm{O}_{10}$	3.882(4)	15.990(3)	241.0
$(\mathrm{CuCl})\mathrm{Ca}_2\mathrm{Ta}_3\mathrm{O}_{10}$	3.829(7)	15.533(2)	227.8
$(\mathrm{CuCl})\mathrm{Ca}_2\mathrm{Nb}_3\mathrm{O}_{10}$	3.844(5)	15.659(6)	231.4

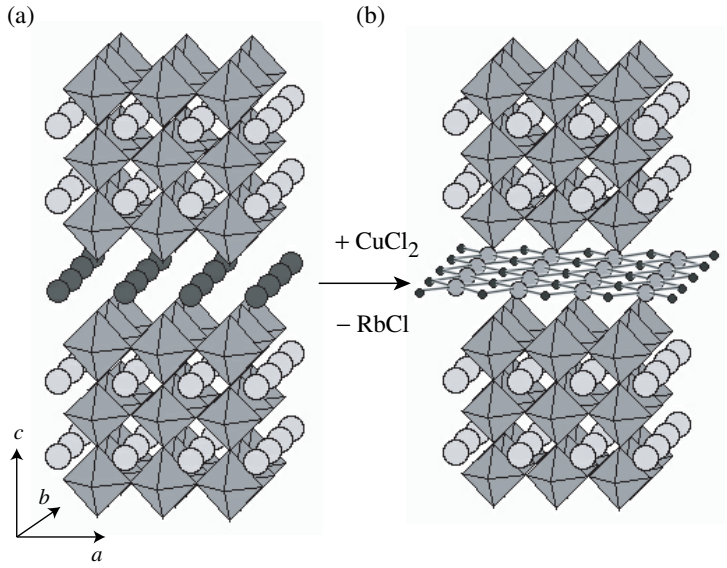

Fig. 1. The ion-exchange reaction of $RbA_2B_3O_{10}$ (A = Ca, Sr; B = Nb, Ta) and $CuCl_2$ for the synthesis of $(CuCl)A_2B_3O_{10}$, where the large dark spheres are rubidiums, the large gray spheres are A cations, the small closed spheres are copper cations, the intermediate gray spheres are chlorines, and the octahedra represent BO_6.

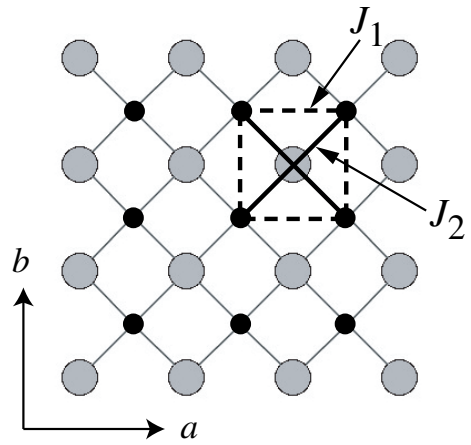

Fig. 2. The CuCl layer viewed along the tetragonal c axis. The bold broken and solid lines represent, respectively, the J_1 and J_2 bonds.

§4. Magnetic properties

Among thus obtained eight compounds, the magnetic properties had been investigated for only three compounds $(CuCl)LaNb_2O_7$,[12),14)] $(CuCl)Ca_2Nb_3O_{10}$[15)] and $(CuCl)Ca_2Ta_3O_{10}$.[16)] In Figs. 5–7, we present the magnetic susceptibilities χ of all the compounds, plotted against temperature. In high temperature region, all the magnetic susceptibilities exhibit the Curie-Weiss behavior, i.e., $\chi = C/(T+\theta)$, with

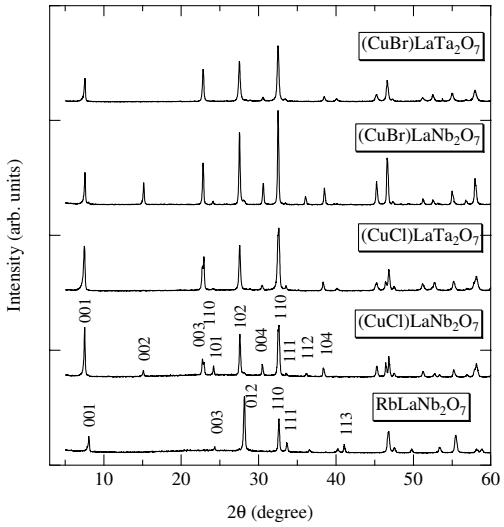

Fig. 3. The X-ray diffraction patterns for the $n = 2$ family (CuX)LaB_2O$_7$ relative to the mother compound RbLaNb$_2$O$_7$.

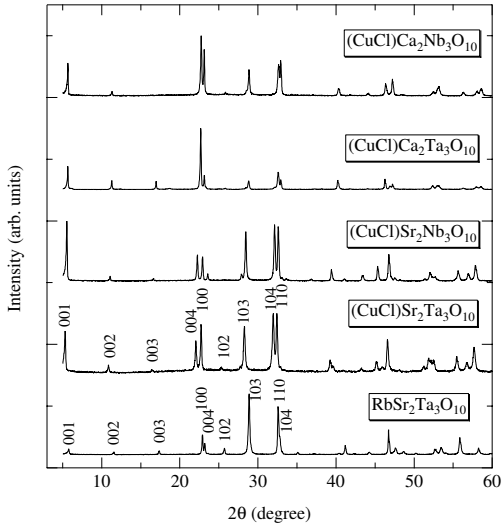

Fig. 4. The X-ray diffraction patterns for the $n = 3$ family (CuCl)A_2B_3O$_{10}$ relative to the mother compound RbSr$_2$Ta$_3$O$_{10}$.

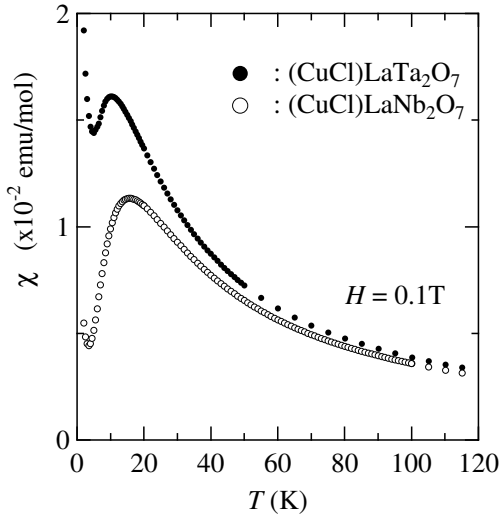

Fig. 5. The temperature variation of magnetic susceptibility for (CuCl)LaNb$_2$O$_7$ and (CuCl)LaTa$_2$O$_7$ measured at $H = 0.1$ T.

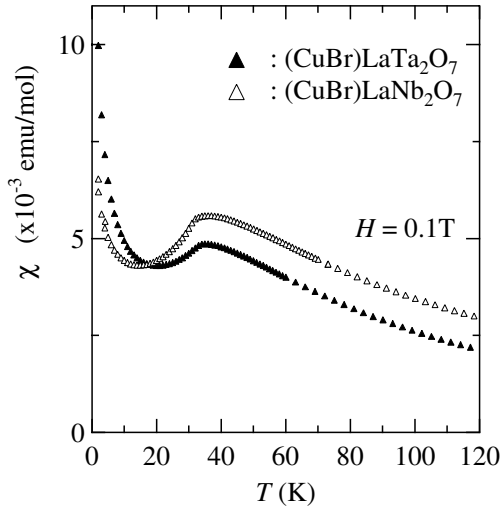

Fig. 6. The temperature variation of magnetic susceptibility for (CuBr)LaNb$_2$O$_7$ and (CuBr)LaTa$_2$O$_7$ measured at $H = 0.1$ T.

the effective magnetic moment being nearly consistent with that expected for $S = 1/2$. In addition, a broad maximum at low temperatures in the χ-T curve is commonly observed (except for the A = Sr case), which is a characteristic feature for the low-dimensional antiferromagnets. It is easy to find a great diversity in the magnetic properties as a function of A, B, X and n. For example, the Weiss temperature θ = 9.6 K for (CuCl)LaNb$_2$O$_7$ is smaller than θ = 15.6 K for (CuCl)LaTa$_2$O$_7$, despite

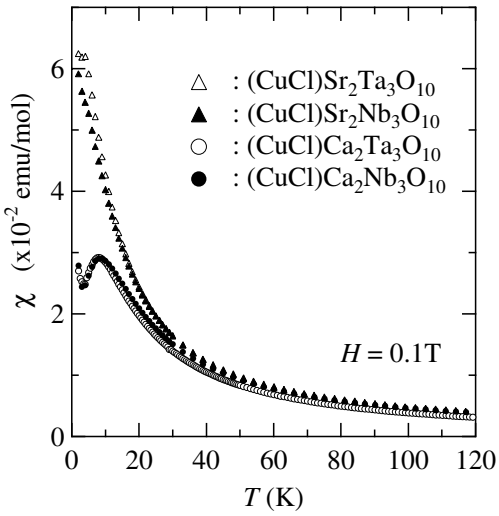

Fig. 7. The temperature variation of magnetic susceptibility for (CuCl)$A_2B_3O_{10}$ (A = Ca, Sr; B = Nb, Ta) measured at H = 0.1 T.

nearly identical unit cell parameters. With lowering temperature, the difference in the χ-T curves between the two compounds become even more distinct as seen in Fig. 5: for (CuCl)$LaNb_2O_7$, χ takes the maximum at 16.5 K ($= T_{\rm max}^{\chi}$) and then drops significantly to zero for $T \rightarrow 0$, apart form the Curie-tail below 5 K due to extrinsic impurity or defects. The thermal-activated behavior indicates that it has a spin-singlet ground state with a finite energy gap. On the contrary, (CuCl)$LaTa_2O_7$ has a somewhat smaller $T_{\rm max}^{\chi}$) of 10.5 K and the reduction of the susceptibility below $T_{\rm max}^{\chi}$) is much smaller. Thus the magnetic ground state is expected for the tantalate. Shown in Fig. 6 are the susceptibilities for (CuBr)LaB_2O_7. Compared with the X = Cl case, the χ-T curves for X = Br exhibit a broad maximum at much higher temperature ($\sim$ 36 K), implying stronger exchange constants via superexchange pathways through bromines. The long-range antiferromagnetic ordering at 31 K is inferred from the curvatures below $T_{\rm max}^{\chi}$). In Fig. 7, the magnetic susceptibilities of the $n = 3$ series are compared. It is interesting to point out that for a given A there is no appreciable difference between susceptibilities of B = Nb and Ta, in contrast to the $n = 2$ case where distinct ground states are expected as mentioned above. The magnetic properties for the $n = 3$ family depend only on A: Although the fits of all the χ-T data in Fig. 7 to the Curie-Weiss law led to similar values of θ =1 $\sim$ 2 K, (CuCl)$Sr_2B_3O_{10}$ shows the Curie-Weiss behavior at least down to 2 K, whereas broad maxima at 8 K are observed for (CuCl)$Ca_2B_3O_{10}$. This may result from the change of both J_1 and J_2 by the expansion of the CuCl plane for A = Sr while keeping the sum of J_1 and J_2 unchanged. At the present moment, it is impossible to give complete explanations about the roles of A, B, X and n in changing the magnetic properties. It would necessary to add other related compounds and also to improve the sample quality.

§5. Spin-singlet ground state in (CuCl)$LaNb_2O_7$

The magnetic susceptibility $\chi_{\rm r}$ of (CuCl)$LaNb_2O_7$ is replotted by the open circles in Fig. 8. By subtracting the Curie-tail below 5 K, one obtains the spin susceptibility $\chi_{\rm s}$ (solid circles). In order to mainly estimate the spin gap Δ, $\chi_{\rm s}$ was analyzed using a $S = 1/2$ isolated AFM dimer model. The value of Δ was determined so as to make $T_{\rm max}^{\chi}$) for $\chi_{\rm s}$ coincide with that for the theoretical susceptibility $\chi_{\rm d}$ (solid line). Thus obtained value of Δ = 26.5 K agrees well with that determined from the neutron scattering experiment (Δ = 26.7 K).[12] The discrepancy between $\chi_{\rm s}$ and $\chi_{\rm d}$ can be

seen around 15 K (Fig. 8) and at high temperatures (Fig. 9). We also tried to use the dimer model to fit χ_s at high temperatures (see broken lines), which however resulted in the marked discrepancy at low temperatures.

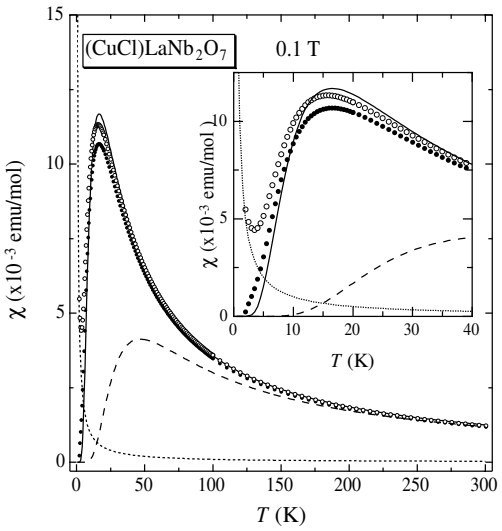

Fig. 8. The temperature dependence of the magnetic susceptibility in (CuCl)$LaNb_2O_7$ measured at $H = 0.1$ T. The open and closed circles represent, respectively, the measured susceptibility χ_r and the spin susceptibility χ_s after subtracting the Curie term (dotted line). The solid and broken lines are the calculated susceptibilities χ_d based on the isolated dimer model with $\Delta = 26.5$ K and 70 K. The enlarged plot is presented in the inset.

From the structural viewpoint, it is natural to consider that the J_1-J_2 model should be the most appropriate model to interpret our experiment. In fact, the chlorines in the CuCl plane are arranged at the center of 2NN bonds, not of 1NN, so that J_2 need not be smaller in magnitude than J_1. Indeed, Cu^{2+}-Cl^{-}-Cu^{2+} angle of 180° for the J_2 bond supports a sizable AFM interaction ($J_2 > 0$) while that of 90° for the J_1 bond points to a ferromagnetic (FM) $J_1(< 0)$. It is known that θ is equal to $J_1 + J_2$ for the J_1-J_2 model. The experimental ratio $T^{\chi}_{max})/\theta_s = 1.65$, much larger than 0.935 for the nonfrustrated case of ($J_1 \ll J_2$ or $J_2 \ll J_1$),[17] indicates ferromagnetic J_1 bonds and the significant frustration due to sizable AFM J_2 bonds. It means that the observed spin-liquid phase is essentially different from that expected for the antiferromagnetic exchanges between the Néel order and collinear phases. Shannon et al. theoretically suggest that there should also be a spin-liquid phase occurring for $J_2/J_1 \sim -0.5$ between the ferromagnetic and collinear ordered phases.[18] We fitted our χ_s data using the high-temperature series expansion developed by Rosner et al.,[19] where $J_1 + J_2$ was fixed to be 10 K. However, as one can see from Fig. 10, the best fit was obtained when J_1 is close to zero, where the long-range ordered state should be stabilized. The deviation of the J_1-J_2 model might suggest possible additional contribution of distant neighbor exchanges such as J_3 and J_4. As an alternative scenario, the effect of disorder of chlorines within the CuCl plane as suggested by the neutron diffraction patterns at room temperature[20] might be seriously taken into account.

§6. Summary

To summarize, we synthesized through the topochemical ion-exchange route a series of magnetic compounds with the general formula $(CuX)A_{n-1}B_nO_{3n+1}$ in which $S = 1/2$ copper ions form the square lattice, separated well by the nonmagnetic perovskite slabs. All compounds show the magnetic behaviors characteristic of low-dimensional antiferromagnets. It should be emphasized that the magnetic properties

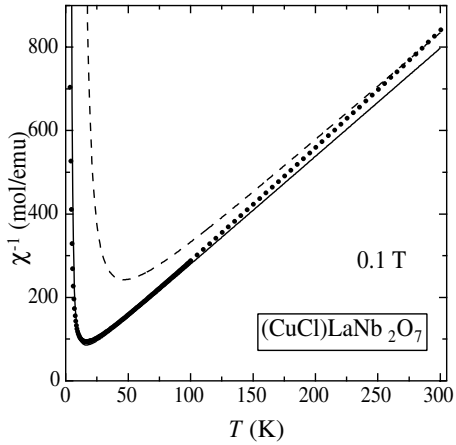

Fig. 9. Reciprocal susceptibilities, $1/\chi_s$ and $1/\chi_d$.

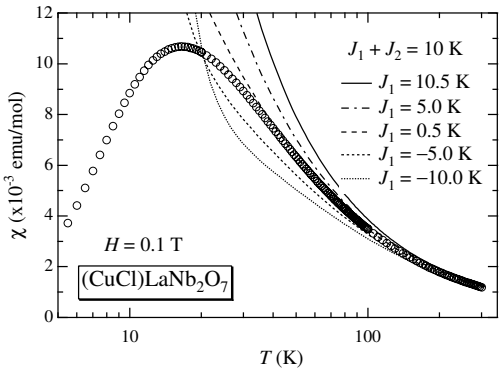

Fig. 10. Comparison between χ_s and those based on the high-temperature series expansion.[19)]

can be tunable with varying A, B, X and n, thus offering the opportunities to study the phase diagram of J_1-J_2 model. In particular, $(CuCl)LaNb_2O_7$ has the spin-singlet ground state with the energy gap of 26.7 K, which should arise from the strong geometrical frustration and quantum fluctuations that destabilize the classical ordering.

Acknowledgements

This work has been partly supported by 21st Century COE Program, Kyoto University Alliance for Chemistry.

References

1) M. Hase, I. Terasaki and K. Uchinokura, Phys. Rev. Lett. **70** (1993), 3651.
2) Y. Ajiro, T. Goto, H. Kikuchi, T. Sakakibara and T. Inami, Phys. Rev. Lett. **63** (1989), 1424.
3) M. Azuma, Z. Hiroi, M. Takano, K. Ishida and Y. Kitaoka, Phys. Rev. Lett. **73** (1994), 2626.
4) J. C. Bonner, S. A. Friedberg, H. Kobayashi and D. L. Meier, Phys. Rev. B **27** (1983), 248.
5) H. Yasuoka, S. Kambe, Y. Itoh and T. Machi, Physica B **199-200** (1994), 278.
6) N. Read and S. Sachdev, Phys. Rev. Lett. **62** (1989), 1694.
7) M. P. Gelfand, R. R. P. Singh and D. A. Huse, Phys. Rev. B **40** (1989), 10801.
8) F. Becca and F. Mila, Phys. Rev. Lett. **89** (2002), 037204.
9) R. Melzi, P. Carretta, A. Lascialfari, M. Mambrini, M. Troyer, P. Millet and F. Mila, Phys. Rev. Lett. **85** (2000), 1318.
10) R. Melzi, S. Aldrovandi, F. Tedoldi, P. Carretta, P. Millet and F. Mila, Phys. Rev. B **64** (2001), 024409.
11) E. E. Kaul, H. Rosner, M. Shannon, R. V. Shpanchenko and C. Geibel, J. Magn. Magn. Mater. **272-276** (2004), 922.
12) H. Kageyama, T. Kitano, N. Oba, M. Nishi, S. Nagai, K. Hirota, L. Viciu, J. B. Wiely, J. Yasuda, Y. Baba, Y. Ajiro and K. Yoshimura, submitted to J. Phys. Soc. Jpn.
13) H. Kageyama, M. Nishi, N. Aso, K. Onizuka, T. Yosihama, K. Nukui, K. Kodama, K.

Kakurai and Y. Ueda, Phys. Rev. Lett. **84** (2000), 5876.
14) T. A. Kodenkandath, J. Lalena, W. L. Zhou, E. Carpenter, C. Sangregorio, A. Falster, W. Simmons, C. O'Connor and J. B. Wiley, J. Am. Chem. Soc. **121** (1999), 10743.
15) T. A. Kodenkandath, A. S. Kumbhar, W. L. Zhou and J. B. Wiley, Inorg. Chem. **40** (2001), 710.
16) H. Kageyama, L. Viciu, G. Caruntu, Y. Ueda and J. B. Wiley, J. of Phys.: Cond. Mat. **16** (2004), S590.
17) J.-K. Kim and M. Troyer, Phys. Rev. Lett. **80** (1998), 2705.
18) N. Shannon, B. Schmidt, K. Penc and P. Thalmeier, Eur. Phys. J. B **38** (2004), 599.
19) H. Rosner, R. R. P. Singh, W. H. Zheng, J. Oitmaa and W. E. Pickett, Phys. Rev. B **67** (2003), 014416.
20) G. Caruntu, T. A. Kodenkandath and J. B. Wiley, Mater. Res. Bull. **37** (2002), 593.